Corrosion Science 106 (2016) 55–60

Contents lists available at ScienceDirect

Corrosion Science

journal homepage: www.elsevier.com/locate/corsci

Corrosion of ternary Mn–Cu–Au to nanoporous Au–Cu with widely tuned Au/Cu ratio for electrocatalyst

X. Li [a], H.-J. Qiu [a,*], J.Q. Wang [b], Y. Wang [a]

[a] The State Key Laboratory of Mechanical Transmissions and School of Chemistry and Chemical Engineering, Chongqing University, Chongqing 400044, China

[b] Ningbo Institute of Material Technology and Engineering, Chinese Academy of Sciences, Ningbo 315201, China

ARTICLE INFO

Article history:
Received 30 September 2015
Received in revised form 22 January 2016
Accepted 27 January 2016
Available online 29 January 2016

Keywords:
A. Alloy
B. SEM
C. De-alloying
C. Oxidation

ABSTRACT

By one-step dealloying a single phase $Au_5Cu_{25}Mn_{70}$ alloy, nanoporous AuCu alloys (np-AuCu) with widely tuned Au:Cu ratio are obtained. The one-step corrosion in $(NH_4)_2SO_4$ solution involves two step dealloying process. The first one is fast dealloying of Mn, resulting in np-$Au_{16}Cu_{84}$. The second step is slow etching of Cu, which is used to tune the ratio of Cu/Au on the AuCu nano-ligament surface. Electrochemical measurements exhibit that the electrocatalytic activities of ultrafine np-AuCu towards glucose oxidation and H_2O_2 reduction depend on the ratios of the Au:Cu. The activities follow the order that np-$Au_{66}Cu_{34}$ > np-$Au_{58}Cu_{42}$ > np-$Au_{78}Cu_{22}$ > np-Au.

1. Introduction

Recently, green energy technologies such as fuel cells/biofuel cells have been attracting great research interest due to their importance for the sustainable development of modern society. Compared with other fuel cells, the fuel cell powered with glucose derived from degradable biomass has received a lot of attention [1–3]. Theoretically, glucose can be completely oxidized to CO_2 and H_2O, releasing 24 electrons per glucose molecule [4]. Therefore, the direct glucose fuel cell is of high energy-density.

For enzyme catalyzed glucose biofuel cells, glucose dehydrogenase (GDH) and glucose oxidase (GOx) are usually used [5–9]. Although these enzyme exhibit high catalytic activity and selectivity, these biocatalysts are lack of long-term stability originating from the intrinsic nature of the enzymes. To address these issues, many attempts have been made to develop catalysts with high activities for glucose electro-oxidation. Early research on this subject has focused on the use of noble metals such as Pt [10] and Au [11]. However, these electrodes lose their activity quickly due to the accumulation of chemisorbed intermediates which block the electrode surface. Nowadays, the fast development of nanotechnology and the appearance of numerous nanostructured materials provide us new opportunities for developing novel nonenzymatic glucose fuel cells [12].

Quite recently, nanostructured Au has also been demonstrated to be an excellent electrocatalyst for glucose oxidation and fabrication of glucose fuel cells and biosensors [13–21]. However, it is noticed that pure Au nanomaterials are used in most of these works and the high cost of pure Au certainly inhibits their commercialization. For practical applications, Au-based alloy nanostructures are more interesting. Moreover, alloying with transition metals has been demonstrated to be an effective strategy to improve the catalytic performance of noble metals by changing their electronic structure as well as the correlating ligand and strain effects [22].

Nanoporous Au (np-Au) catalyst prepared by alloy corrosion has attracted much attention during the last decade [23,24]. It is known that uniform np-Au prepared by dealloying single phase binary precursors (such as AuAg or AuCu alloys) usually contains a very low amount of non-noble metals (usually less than 15 at.%) [24]. To prepare np-Au with a high and tunable non-noble metal content, ternary precursors are more promising considering that the most active component can be selectively removed and the content of the other two components can be precisely controlled [25]. In our previous work, we have proposed Al-based ternary systems such as Pd–Cu–Al ternary alloys to demonstrate this concept [26]. However, most of these Al-based ternary precursors contain multiple intermetallic phases, which would obviously affect the uniformity and alloy quality of the resulting nanoporous alloys [26,27]. Al-based single phase ternary alloys has also been reported with

* Corresponding author.
E-mail addresses: hjqiu@cqu.edu.cn (H.-J. Qiu), jqwang@nimte.ac.cn (J.Q. Wang), wangy@cqu.edu.cn (Y. Wang).

http://dx.doi.org/10.1016/j.corsci.2016.01.025
0010-938X/

limited composition such as $Al_{66}Au_{27.2}Ni_{6.8}$, and $Al_{66}Au_{27.2}Co_{6.8}$ [28]. The design of single phase ternary precursors which is tunable in composition and suitable for selective etching is still very challenging. In this work, we design a single phase Mn–Cu–Au ternary precursor which can be selectively and step by step dealloyed (Mn first then Cu) to fabricate nanoporous binary Au–Cu alloys with widely tuned Cu/Au surface ratio. Electrochemical measurements show that the nanoporous AuCu alloy (np-AuCu) exhibits high and composition-depended electrocatalytic activity towards glucose oxidation and H_2O_2 reduction.

2. Experimental

$Au_5Cu_{25}Mn_{70}$ alloy with a thickness of ~30 μm and a width of ~3 mm were made by refining pure Mn, Au and Cu (>99.9%) in an arc furnace under the protection of argon, followed by melt-spinning. Nanoporous AuCu alloys with tunable Au/Cu ratios were prepared by chemical dealloying the precursor for different times in 1 M $(NH_4)_2SO_4$ solution (not deaerated) at room temperature.

Powder X-ray diffraction (XRD) data were collected on a Bruker D8 advanced X-ray diffractometer using Cu Kα radiation (λ = 1.5418 Å). The microstructures were characterized on a JEM-2100 high-resolution transmission electron microscope (TEM) and a JEOL JSM-6700F field emission scanning electron microscope (SEM) equipped with an Oxford INCA X-sight energy dispersive X-ray spectrometer (EDS). For the TEM characterization, the np-AuCu was ultra-sonicated in ethanol forming a suspension. Several drops of the suspension were then dropped on a Cu screen substrate and dried overnight at room temperature. For the SEM characterization, one piece of np-AuCu (~3 mm × 3 mm) was immobilized on the Cu substrate using a conductive carbon tape.

All electrochemical tests were performed on a CHI 660E electrochemical workstation at room temperature. A three-electrode system was used with the dealloyed nanoporous metal as working electrode, Pt foil as counter electrode, and saturated calomel electrode (SCE) as reference electrode. The np-AuCu catalyst suspensions were made by mixing np-AuCu (3.0 mg), carbon powder (4.0 mg), ethanol (300 μL), and Nafion solution (0.5 wt.%, 100 μL) under sonication for 20 min. The working electrode was prepared by dropping the suspension (4 μL) on a glassy carbon electrode. The electrolyte for the electrochemical test was 0.2 M NaOH solution with or without 50 mM glucose. For the Cyclic Voltammetry (CV) test, the scan rate is 50 mV s^{-1}. Current-time curves were recorded at 0.2 V in 0.2 M NaOH aqueous solution with and without addition of 1 mM glucose (each time). During the whole current-time testing process, the electrolyte was stirred using a magnetic stirring equipment. Before each test, the electrolytes were deoxygenated with high-purity N_2 for 20 min.

3. Results and discussion

3.1. Preparation and characterization of np-AuCu alloys

Normally, np-Au dealloyed from binary alloys such as AuAg and AuCu alloys only contains a few atomic percentage of residual Ag or Cu. In order to lower the catalyst cost and possibly enhance the catalytic activity, in this work, we try to prepare np-AuCu alloys with widely tuned surface composition by dealloying a ternary $Au_3Cu_{22}Mn_{75}$ precursor.

The composition of the precursor is controlled by the feed ratio of each element and also confirmed by EDS analysis (data not shown). The XRD pattern of the precursor shows three main peaks locating at ~41.2, 47.9, and 70.0°, which can be assigned to (1 1 1), (2 0 0) and (2 2 0) diffraction of a single phase face-centered cubic (fcc) structure (Fig. 1a). The XRD pattern of the resulted sample

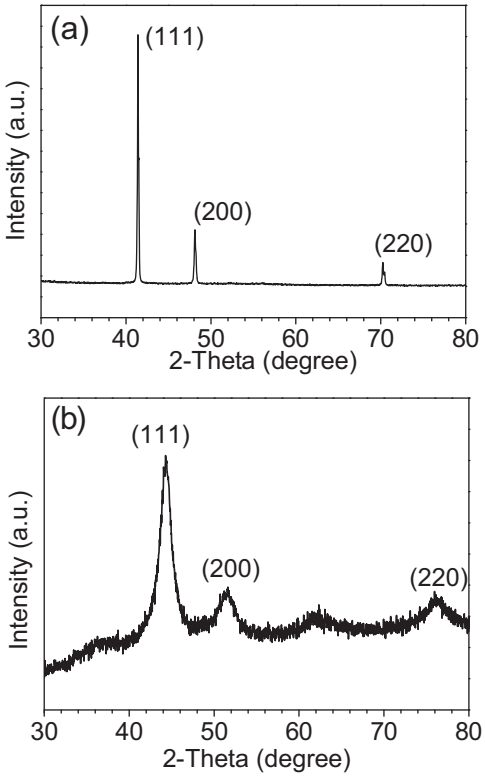

Fig. 1. XRD patterns of the ternary $Au_5Cu_{25}Mn_{70}$ alloy before (a) and after (b) dealloying in 1 M $(NH_4)_2SO_4$ solution for 2 days.

after the dealloying of Mn is shown in Fig. 1b. The three diffraction peaks from the precursor alloy disappear and a new set of three peaks around 44.3, 51.5, and 76.2° appears. Compared with the peaks from the precursor, these new peaks become broad and shift to higher degree, suggesting the formation of nanoscale crystals and the removal of Mn with a bigger atomic size, respectively [25]. Besides the three main peaks, two small diffraction peaks at 36 and 62° can be assigned to Cu_2O which is formed by the oxidation of nanoscale surface Cu in air. Thus, the final product is actually np-AuCu/Cu_2O composite. It is found that after the removal of Mn (bubbling stopped), the Cu content can be further tuned by extending the dealloying time in the same $(NH_4)_2SO_4$ dealloying solution. For example, the AuCu ratio of np-$Au_{16}Cu_{84}$ (after just removal of Mn) can be tuned to be around $Au_{66}Cu_{34}$, $Au_{58}Cu_{42}$, $Au_{78}Cu_{22}$, $Au_{97}Cu_3$, respectively, after dealloying for 2, 3, 7, and 10 days. The EDS spectrum of each sample is shown in Fig. S1 in Supporting information.

Fig. 2a shows a low magnification section-view SEM image of np-$Au_{58}Cu_{42}$. It is observed that the free-standing nanoporous alloy is very uniform and has a thickness of ~30 μm. The zoom-in SEM image in Fig. 2b shows that the np-AuCu has a spongy-like bicontinuous ligament-pore nanostructure with a small ligament size of less than 10 nm. Fig. 2c gives the corresponding TEM image, in which the color contrast between the dark ligaments and bright pores further indicates the formation of interpenetrating ultrafine ligament/pore structure. We can also observe some thin film-like material covering the nanoligaments (indicated by arrows in Fig. 2c). These thin films can be assigned to the formed Cu_2O by oxidation in air, which is also confirmed by the selective area electron diffraction (SAED) image in Fig. S2. The HRTEM image (Fig. 2d) of the sample shows that ordered lattice fringes are well resolved around the bright pore. The lattice distance is calculated to be ~0.2 nm, corresponding to the distance of the (111) crystal plane of fcc AuCu alloy. When comparing the nanoporous structure (ligament/pore

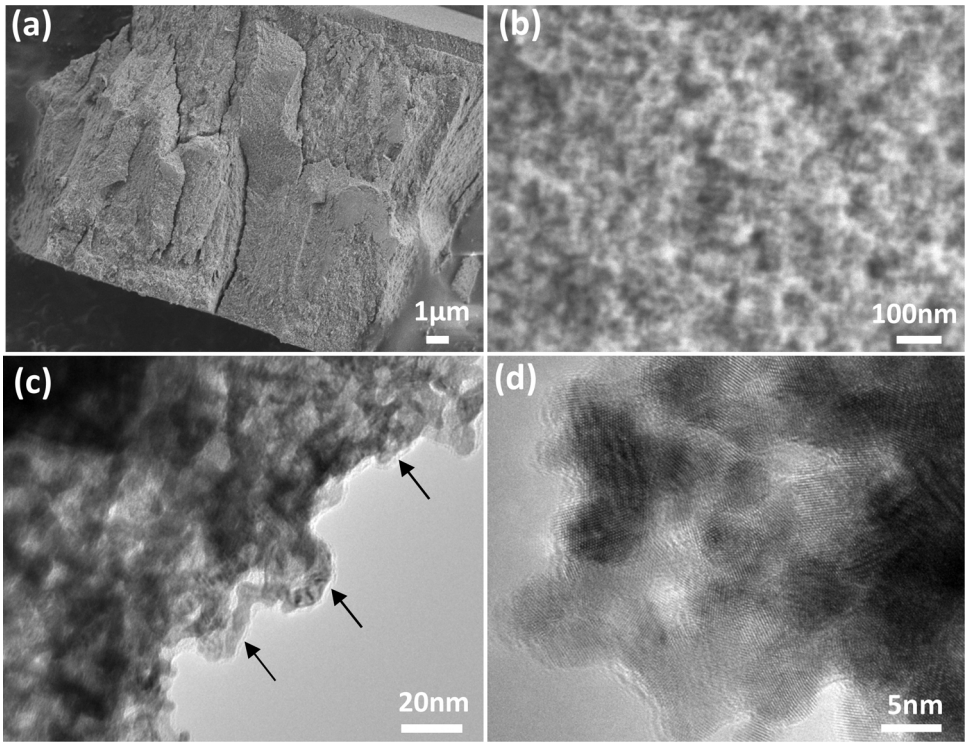

Fig. 2. SEM (a, b), TEM (c) and HRTEM (d) images of dealloyed np-AuCu alloy (2-day dealloying).

size: ~25 nm) obtained by dealloying $Mn_{70}Cu_{30}$ alloy (Fig. S3), the nanopore/ligament size of np-AuCu is much smaller (~10 nm). This result suggests that the addition of Au in the $Mn_{70}Cu_{30}$ precursor can significantly inhibit the fast diffusion of Cu during the dealloying of Mn. The inhibition effect has been frequently observed from metals with low surface diffusivity such as Pt and Pd [25,26]. In this work, it is found that Au which has a relatively fast surface diffusivity [29] can also greatly inhibit the diffusion rate of a fast-diffusion metal such as Cu, resulting in an ultrafine nanoporous structure. It should be noted that further dissolution of Cu from the np-$Au_{16}Cu_{84}$ has no observable effect on the nanoporous structure although theoretically it would increase the porosity of the nanoporous structure since more Cu are removed.

3.2. Electrocatalytic activities of np-AuCu towards glucose oxidation

The electrocatalytic activities of the np-AuCu alloys/composites towards glucose oxidation are examined to evaluate their potential application in glucose fuel cells or electrochemical sensing. Fig. 3a shows the CV profiles of np-AuCu in the 0.2 M NaOH solution. In the blank NaOH solution, the peaks at a potential of −0.4 V and −0.2 V is due to the oxidation of Cu into Cu(I) and Cu(II), respectively [30]. The current over 0 V should be caused by the oxidation of some Cu(II) to Cu(III) and the oxidation of Au [30,31]. As observed that these peaks also appear from pure Cu electrode (Fig. 3b). During the negative scan, the peak at ~−0.2 V is assigned to the reduction of Au–OH into Au. The peaks at −0.5 V and −0.8 V is due to the reduction of Cu(II) to Cu(I) and Cu(0), respectively. It is also observed that when most Cu has been removed ($Au_{97}Cu_3$), the sample shows a typical electrochemical behaviour of Au and the peaks from Cu can be barely observed. After the addition of 50 mM glucose (Fig. 3c) in the NaOH aqueous solution, in the positive scan, the first increase in current (starts from ~−0.8 V) could be due to glucose electro-adsorption and generation of adsorbed intermediates (per glucose molecule lost one proton in this electrochemical reaction) [31]. When the applied potential is larger than 0 V, Au–OH species are generated in the alkaline solution. Au–OH is beneficial in oxidizing the intermediates derived from the glucose electro-adsorption. This process also releases free active Au sites for the direct oxidation of glucose resulting in a big current peak at ~0.2–0.4 V. Since CuO is also very active for the oxidation of glucose [32–34], the formation of Cu(II) should also contribute to the high catalytic activity of the np-AuCu catalysts. The current decrease after the peak should be attributed to the formation of Au oxides which block the active Au sites for glucose oxidation [31]. In the negative scan, the oxidation of glucose is suppressed due to the oxidized Au surface. The oxidized Au surface begins to be reduced at a potential ~0.2 V, and its activity starts to show some recovery, resulting in a large anodic peak at ~0-0.2 V. Since at this potential some Cu(III) has also been reduced to Cu(II), the second anodic peak (at ~-0.2 V) may be due to the oxidation of glucose on the generated Cu(II) surface.

As also observed from Fig. 3c, the four np-AuCu samples show similar electrochemical behavior for glucose oxidation. However, the surface-specific current densities for glucose electro-oxidation are clearly different with np-$Au_{66}Cu_{34}$ exhibiting the largest current density. The highest current density at np-$Au_{66}Cu_{34}$ should result from the optimized surface Au/Cu composition of this sample towards glucose oxidation. The inclusion of a certain amount of Cu may cause an alloy effect, and modified surface strain, resulting in an enhanced catalytic activity [35]. Moreover, the coexistence of Au and Cu_2O/CuO surface during the electrochemical reaction clearly results in a synergistic catalytic effect for the oxidation of glucose since all these AuCu alloy sample exhibit higher catalytic activity compare with the almost pure Au sample ($Au_{97}Cu_3$).

For practical fuel applications, the electrocatalytic durability of catalyst is very important. As shown in Fig. 3d, the glucose electro-oxidation at the np-$Au_{66}Cu_{34}$ alloy is fairly stable because the features of the CV curves remain almost unchanged after 200CV cycles in 0.2 M NaOH + 50 mM glucose solution. In addition, no obvious change is detected after the electrode has been stored at 4 °C for

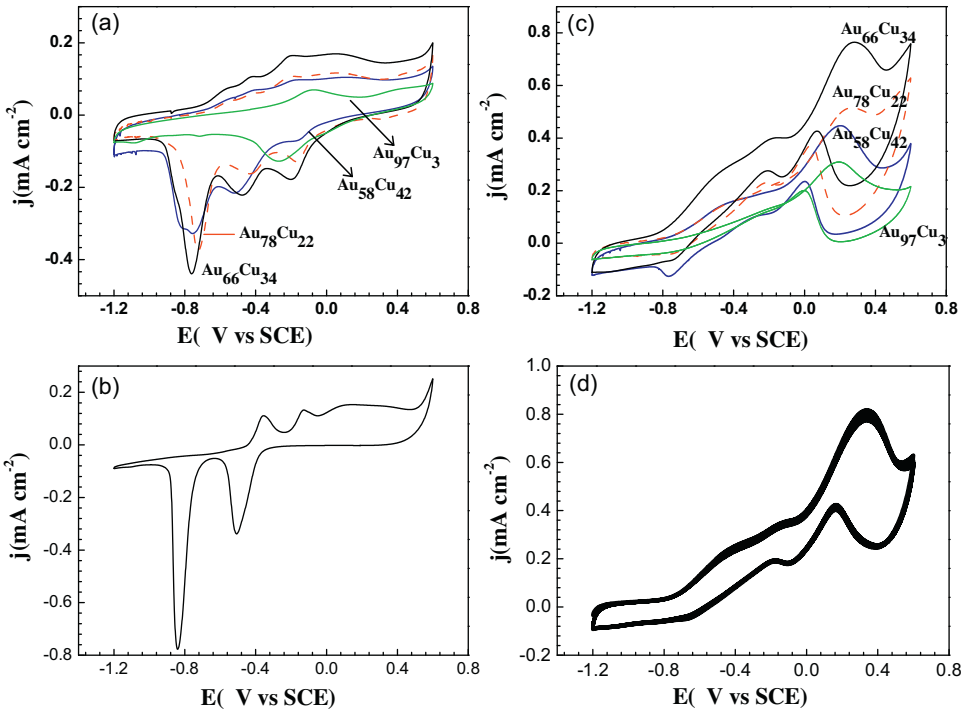

Fig. 3. CV curves of np-AuCu in 0.2 M NaOH solution without (a) and with (c) 50 mM glucose; CV curves of pure Cu in 0.2 M NaOH aqueous solution (b); CV curves (200CV cycles) of np-$Au_{66}Cu_{34}$ alloy in 0.2 M NaOH + 50 mM glucose solution (d). Scan rate are 50 mV s^{-1} for all the tests.

four weeks. These results indicate that the np-AuCu alloy catalysts have a good catalytic and storage stability.

For potential electrochemical sensing applications, electrocatalysts are usually evaluated by measuring current response vs. time at a certain potential after the addition of analyte. Fig. 4a shows the current response of the np-$Au_{66}Cu_{34}$ electrode with and without the addition of 1 mM glucose. It is clear that after the addition of glucose, the current increases dramatically, indicating the oxidation of glucose at this applied potential (0.2 V). Fig. 4b shows the current response of the electrode towards the successive addition of 1 mM glucose at 0.2 V. For comparison, the response of np-$Au_{97}Cu_3$ under the same condition has also been included. After the addition of glucose, the current responses more sensitively at np-$Au_{66}Cu_{34}$ and reaches ~97% of the steady state value within 3 s. The response time is similar to those obtained at Pd-SWNTs (3 s) [14] and porous gold (2 s) [36] electrodes. However, it is much shorter than those at Pd/epoxy–Ag (6 s) [15] and Pb-graphene (9 s) [16] electrodes, suggesting that the np-AuCu electrode responds rapidly to the change of glucose concentration. The fast response can be attributed to the fact that glucose can diffuse freely into the 3D bicontinuous nanoporous structure and the enhanced catalytic activity. As shown in Fig. 4c, the electrode responds linearly to glucose over a wide concentration range (0–12 mM, $R = 0.997$) with a sensitivity of ~50 μA mM^{-1} cm^{-2}.

3.3. Electrocatalytic activities of np-AuCu towards H_2O_2 reduction

Besides acting as an anodic electrocatalyst, we also test the present np-AuCu for H_2O_2 electro-reduction, which is an important fuel cell cathode reaction. As shown in Fig. S4, all the three catalysts tested are very active for H_2O_2 reduction. At potential of −0.3 V, the np-$Au_{66}Cu_{34}$ catalyst clearly exhibits a higher current for the H_2O_2 reduction. Compared with np-$Au_{58}Cu_{42}$, the np-$Au_{66}Cu_{34}$ shows a much higher reduction current between 0 and −0.6 V. Compared with np-$Au_{78}Cu_{22}$, the np-$Au_{66}Cu_{34}$ shows a higher current at potential between 0 and −0.3 V. Between −0.3 V and −0.6 V, however, the np-$Au_{78}Cu_{22}$ also shows a similar high current since Au becomes very active for H_2O_2 reduction at this potential range [37]. Therefore, the np-$Au_{66}Cu_{34}$ catalyst exhibits overall the best performance for the electro-reduction of H_2O_2. Again, the best performance should be owing to a suitable Au/Cu ratio which would result in an optimum Au and Cu_2O surface composition and surface strain for the electro-catalyzed reaction.

It is also worth mentioning that this fabrication strategy i.e., dealloying Mn-based ternary alloys, can also be extended to prepare other nanoporous alloys with tunable compositions, such as np-PtCu, and np-NiCu alloys, or nanoporous composites, such as np-NiCu/$NiCuO_x$. Fig. S5 shows the SEM images of np-PtCu and np-NiCu alloys obtained by dealloying $Pt_5Cu_{20}Mn_{75}$ and $Ni_5Cu_{20}Mn_{75}$, respectively. It is observed that as expected, the addition of Pt and Ni greatly inhibit the surface diffusivity of Cu during the dealloying process, resulting in ultrafine nanoporous structures. These nanoporous alloys with tunable compositions and uniform structure should be very useful for other important applications [38,39].

4. Conclusions

Free-standing np-AuCu alloys with uniform ligament-pore size and controllable bimetallic Au/Cu ratio are facilely fabricated by a dealloying process. Electrochemical measurements demonstrate that the np-$Au_{66}Cu_{34}$ alloy exhibits greatly enhanced electrocatalytic activity and durability towards glucose oxidation and H_2O_2 reduction compared with other np-AuCu samples. Owing to the excellent electrocatalytic activity, the np-$Au_{66}Cu_{34}$ also responses sensitively towards the addition of glucose. These results indicate that the prepared np-AuCu alloy is promising as both anode and cathode catalyst for glucose fuel cells.

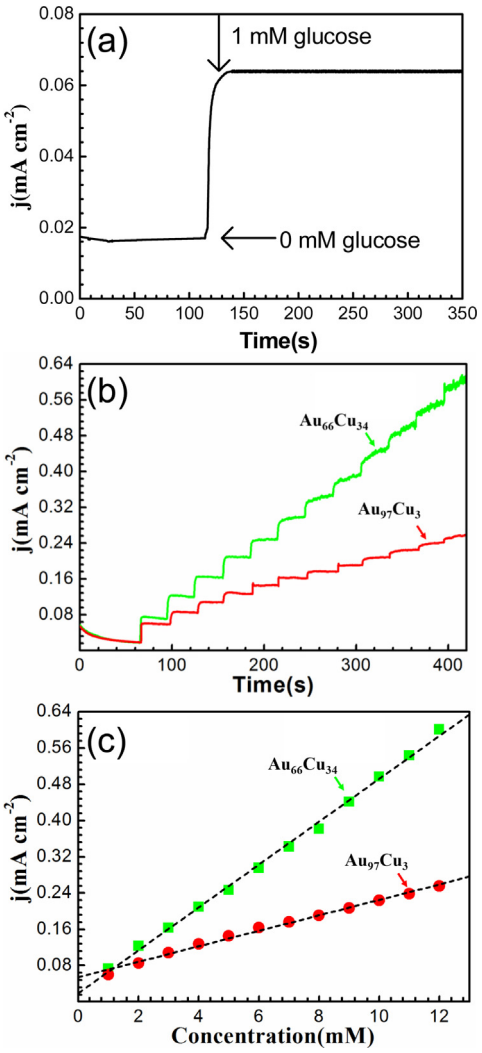

Fig. 4. Current-time curves of np-$Au_{66}Cu_{34}$ alloy in a stirred 0.2 M NaOH solution before and after addition of 1 mM glucose at 0.2 V (a); continuous addition of glucose (1 mM) under 0.2 V (b); (c) is the calibration curve of glucose on this electrode.

Acknowledgements

Financial support is from Chongqing Basic and Frontier Research Project (cstc2015jcyjA50026), Thousand Young Talents Program of the Chinese Central Government (No. 0220002102003), National Natural Science Foundation of China (NSFC, No. 21373280), and Hundred Talents Program at Chongqing University (No. 0903005203205).

Appendix A. Supplementary data

Supplementary data associated with this article can be found, in the online version, at http://dx.doi.org/10.1016/j.corsci.2016.01.025.

References

[1] Y. Zhao, L. Fan, Y. Zhang, Q. Que, B. Hong, Three-dimensional Pt_xNi_{1-x} nanoclusters supported on multiwalled carbon nanotubes in enzyme-free glucose biofuel cells, J. Power Sources 296 (2015) 30–39.
[2] A. Kloke, C. Köhler, R. Zengerle, S. Kerzenmacher, Porous platinum electrodes fabricated by cyclic electrodeposition of PtCu alloy: application to implantable glucose fuel cells, J. Phys. Chem. C 116 (2012) 19689–19698.
[3] K.P. Prasad, Y. Chen, P. Chen, Three-dimensional graphene-carbon nanotube hybrid for high-performance enzymatic biofuel cells, ACS Appl. Mater. Interfaces 6 (2014) 3387–3393.
[4] Z.N. Liu, L.H. Huang, L.L. Zhang, H.Y. Ma, Y. Ding, Electrocatalytic oxidation of D-glucose at nanoporous Au and Au–Ag alloy electrodes in alkaline aqueous solutions, Electrochim. Acta 54 (2009) 728 6–7293.
[5] J. Wang, Electrochemical glucose biosensors, Chem. Rev. 108 (2008) 814–825.
[6] Y. Peng, C.-W. Wei, Y.-N. Liu, J. Li, Nafion coating the ferrocenylalkanethiol and encapsulated glucose oxidase electrode for amperometric glucose detection, Analyst 136 (2011) 4003–4007.
[7] K. Dawson, M. Baudequin, A. O'Riordan, Single on-chip gold nanowires for electrochemical biosensing of glucose, Analyst 136 (2011) 4507–4513.
[8] A.H. Liu, H.R. Geng, C.X. Xu, H.J. Qiu, A three-dimensional hierarchical nanoporous PdCu alloy for enhanced electrocatalysis and biosensing, Anal. Chim. Acta 703 (2011) 172–178.
[9] Y. Chen, P. Gai, J. Zhang, J.-J. Zhu, Design of an enzymatic biofuel cell with large power output, J. Mater. Chem. A 3 (2015) 11511–11516.
[10] Y.B. Vassilyev, O.A. Khazova, N.N. Nikolaeva, Kinetics and mechanism of glucose electrooxidation on different electrode-catalysts.1. Adsorption and oxidation on platinum, J. Electroanal. Chem. 196 (1985) 105–125.
[11] R.R. Adzic, M.W. Hsiao, E.B. Yeager, Electrochemical oxidation of glucose on single-crystal gold surfaces, J. Electroanal. Chem. 260 (1989) 475–485.
[12] S.Q. Ci, Z.H. Wen, S. Mao, Y. Hou, S.M. Cui, Z. He, J.H. Chen, One-pot synthesis of high-performance Co/graphene electrocatalysts for glucose fuel cells free of enzymes and precious metals, Chem. Commun. 51 (2015) 9354–9357.
[13] X.M. Chen, Z.J. Lin, D.J. Chen, T.T. Jia, Z.M. Cai, X.R. Wang, X. Chen, G.N. Chen, M. Oyama, Nonenzymatic amperometric sensing of glucose by using palladium nanoparticles supported on functional carbon nanotubes, Biosens. Bioelectron. 25 (2010) 1803–1808.
[14] L. Meng, J. Jin, G.X. Yang, T.H. Lu, H. Zhang, C.X. Cai, Nonenzymatic electrochemical detection of glucose based on palladium-single-walled carbon nanotube hybrid nanostructures, Anal. Chem. 81 (2009) 7271–7280.
[15] A. Gutes, C. Carraro, R. Maboudian, Nonenzymatic glucose sensing based on deposited palladium nanoparticles on epoxy-silver electrodes, Electrochim. Acta 56 (2011) 5855–5859.
[16] L.M. Lu, H.B. Li, F.L. Qu, X.B. Zhang, G.L. Shen, R.Q. Yu, In situ synthesis of palladium nanoparticle-graphene nanohybrids and their application in nonenzymatic glucose biosensors, Biosens. Bioelectron. 26 (2011) 3500–3504.
[17] S.C. Hui, J. Zhang, X.J. Chen, H.H. Xu, D.F. Ma, Y.L. Liu, B.R. Tao, Study of an amperometric glucose sensor based on Pd–Ni/SiNW electrode, Sensor Actuat. B: Chem. 155 (2011) 592–597.
[18] J. Shi, P.L. Ci, F. Wang, H. Peng, P.X. Yang, L.W. Wang, S.L. Ge, Q.J. Wang, P.K. Chu, Nonenzymatic glucose sensor based on over-oxidized polypyrrole modified Pd/Si microchannel plate electrode, Biosens. Bioelectron. 26 (2011) 2579–2584.
[19] F.J. Miao, B.R. Tao, L. Sun, T. Liu, J.C. You, L.W. Wang, P.K. Chu, Amperometric glucose sensor based on 3D ordered nickel-palladium nanomaterial supported by silicon MCP array, Sensor Actuat. B: Chem. 141 (2009) 338–342.
[20] X. Zhong, R. Yuan, Y. Chai, In situ spontaneous reduction synthesis of spherical Pd@Cys-C60 nanoparticles and its application in nonenzymatic glucose biosensors, Chem. Commun. 48 (2012) 597–599.
[21] X.Y. Lang, H.Y. Fu, C. Hou, G.F. Han, P. Yang, Y.B. Liu, Q. Jiang, Nanoporous gold supported cobalt oxide microelectrodes as high-performance electrochemical biosensors, Nat. Commun. 4 (2013) 2169.
[22] C.W. Yi, K. Luo, T. Wei, D.W. Goodman, The composition and structure of Pd–Au surfaces, J. Phys. Chem. B 109 (2005) 18535–18540.
[23] H.J. Qiu, H.-T. Xu, L. Liu, Y. Wang, Correlation of the structure and applications of dealloyed nanoporous metals in catalysis and energy conversion/storage, Nanoscale 7 (2015) 386–400.
[24] H.J. Qiu, L. Peng, X. Li, H.T. Xu, Y. Wang, Using corrosion to fabricate various nanoporous metal structure, Corros. Sci. 92 (2015) 16–31.
[25] H.J. Qiu, H.T. Xu, X. Li, J.Q. Wang, Y. Wang, Core–shell-structured nanoporous PtCu with high Cu content and enhanced catalytic performance, J. Mater. Chem. A 3 (2015) 7939–7944.
[26] C. Xu, H. Geng, H. Qiu, Nanoporous PdCu alloy for formic acid electro-oxidation, J. Power Sources 199 (2012) 124–131.
[27] Z. Zhang, Y. Wang, Z. Qi, C. Somsen, X. Wang, C. Zhao, Fabrication and characterization of nanoporous gold composites through chemical dealloying of two phase Al–Au alloys, J. Mater. Chem. 19 (2009) 6042–6050.
[28] Z. Zhang, C. Zhang, Y. Gao, J. Frenzel, J. Sun, G. Eggeler, Dealloying strategy to fabricate ultrafine nanoporous gold-based alloys with high structural stability and tunable magnetic properties, Crystengcomm 14 (2012) 8292–8300.
[29] Z. Zhang, Y. Wang, Z. Qi, W. Zhang, J. Qin, J. Frenzel, Generalized fabrication of nanoporous metals (Au, Pd Pt. Ag, and Cu) through chemical dealloying, J. Phys. Chem. C 113 (2009) 12629–12636.
[30] H. Qiu, L. Lu, L. Xue, X. Huang, Facile electrochemical preparation of three-dimensional porous Cu films by potential perturbation, Electrochim. Acta 55 (2010) 6081–6087.
[31] H. Qiu, X. Huang, Effects of Pt decoration on the electrocatalytic activity of nanoporous gold electrode toward glucose and its potential application for constructing a nonenzymatic glucose sensor, J. Electroanal. Chem. 643 (2010) 39–45.
[32] C. Dong, H. Zhong, T. Kou, J. Frenzel, G. Eggeler, Z. Zhang, Three-dimensional Cu foam-supported single crystalline mesoporous Cu_2O nanothorn arrays for ultra-highly sensitive and efficient nonenzymatic detection of glucose, ACS Appl. Mater. Interfaces (2015).
[33] J. Song, L. Xu, C. Zhou, R. Xing, Q. Dai, D. Liu, H. Song, Synthesis of graphene oxide based CuO nanoparticles composite electrode for highly enhanced

nonenzymatic glucose detection, ACS Appl. Mater. Interfaces 5 (2013) 12928–12934.
[34] Y. Guo, Y.-T. Xu, B. Zhao, T. Wang, K. Zhang, M.M.F. Yuen, X.-Z. Fu, R. Sun, C.-P. Wong, Urchin-like Pd@CuO–Pd yolk–shell nanostructures: synthesis, characterization and electrocatalysis, J. Mater. Chem. A 3 (2015) 13653–13661.
[35] H.J. Qiu, X. Shen, J.Q. Wang, A. Hirata, T. Fujita, Y. Wang, M.W. Chen, Aligned nanoporous Pt–Cu bimetallic microwires with high catalytic activity toward methanol electrooxidation, ACS Catal. 5 (2015) 3779–3785.
[36] Q. Shen, L. Jiang, H. Zhang, Q. Min, W. Hou, J.-J. Zhu, Three-dimensional dendritic Pt nanostructures: sonoelectrochemical synthesis and electrochemical applications, J. Phys. Chem. C 112 (2008) 16385–16392.
[37] S. Liu, B. Yu, F. Li, Y. Ji, T. Zhang, Coaxial electrospinning route to prepare Au-loading SnO_2 hollow microtubes for non-enzymatic detection of H_2O_2, Electrochim. Acta 141 (2014) 161–166.
[38] Z. Zhao, J. Xu, C. Shang, R. Ye, Y. Wang, Dealloying-driven synthesis of sea-urchin like titanate nanowires and hierarchically porous anatase TiO_2 nanospindles with enhanced photocatalytic performance, Corros. Sci. 98 (2015) 651–660.
[39] H.-J. Qiu, J.Q. Wang, P. Liu, Y. Wang, M.W. Chen, Hierarchical nanoporous metal/metal-oxide composite by dealloying metallic glass for high-performance energy storage, Corros. Sci. 96 (2015) 196–202.